Liquid Crystals
Publication details, including instructions for authors and subscription information:
http://www.informaworld.com/smpp/title~content=t713926090

Selection of droplet size and the stability of nematic emulsions

M. Heppenstall-Butler[a]; A. -M. Williamson[a]; E. M. Terentjev[b]
[a] Unilever Research, Colworth House, Sharnbrook MK44 1LQ, UK [b] Cavendish Laboratory, University of Cambridge, Cambridge, CB3 0HE, UK

To cite this Article Heppenstall-Butler, M. , Williamson, A. -M. and Terentjev, E. M.(2005) 'Selection of droplet size and the stability of nematic emulsions', Liquid Crystals, 32: 1, 77 — 84
To link to this Article: DOI: 10.1080/02678290412331328009
URL: http://dx.doi.org/10.1080/02678290412331328009

Liquid Crystals, Vol. 32, No. 1, January 2005, 77–84

Taylor & Francis
Taylor & Francis Group

Selection of droplet size and the stability of nematic emulsions

M. HEPPENSTALL-BUTLER†, A.-M. WILLIAMSON† and E.M. TERENTJEV*‡
†Unilever Research, Colworth House, Sharnbrook MK44 1LQ, UK
‡Cavendish Laboratory, University of Cambridge, Cambridge, CB3 0HE, UK

(*Received 12 April 2004; accepted 20 September 2004*)

The topological stability of emulsions of thermotropic nematic liquid crystal dispersed in water is examined for a wide range of materials and concentrations. There is a characteristic size of emulsion droplets, $R^*=K/W$, determined by the ratio of Frank elastic, K, and surface anchoring, W, energies of the liquid crystal. Nematic droplets below this size are not topologically charged and coalesce freely. Droplets with $R>R^*$ possess a topological charge +1 and present a high elastic energy barrier for coalescence. We studied the evolution of droplet size distribution with time, illustrating their accumulation in the narrow region around R^*, and the dependence of the droplet size distribution on temperature and type of surfactant that controls the director anchoring on droplet inner surfaces.

1. Introduction

The physics and chemistry of colloids and emulsions are rapidly evolving from the empirical domain of paint design and food technology into an important area of fundamental research [1]. The reason for this is a range of new application possibilities and benefits generated by fundamental studies of complex fluids with internal degrees of freedom and symmetry breaking. At the same time, more clear, challenging and wide-ranging fundamental problems are continually emerging in this area. In particular, the problem of controlled encapsulation and release is clearly of paramount importance to a wide range of applications—from pharmaceuticals to foods and personal products.

When two immiscible fluids are thoroughly blended together, an emulsion is formed (or a colloid suspension, when the characteristic viscosity of the encapsulated fluid is much greater than that of a suspending matrix). The best known examples are, of course, oil-in-water or water-in-oil emulsions. There is an understanding, quite general for colloids and emulsions, that their structural stability is a kinetic concept and not a thermodynamic one [2]. Some emulsions have only a short lifetime before complete phase separation, whereas others remain kinetically stable for years. In order to prepare a stable emulsion there must be a surface active material present to protect the newly formed droplets from immediate coalescence. Such *surfactant* molecules, typically, have two distinct parts—hydrophobic and hydrophilic for oil/water interfaces. By aggregating on such interfaces they reduce the surface tension and, when such a reduction is complete, a microemulsion, i.e. a solution of microscopic micelles, is formed. That state represents a truly thermodynamically stable phase, as opposed to the kinetic stability of macroscopic droplets. The argument is simple: if the surface tension of the interface covered with surfactant is very small ('zero' for practical purposes), the entropy preference of having many small particles in favour of the few big ones makes the molecular-size micelles a ground state of the total free energy. If, on the other hand, the local surface tension is considerable, the configurational entropy becomes irrelevant and the minimum surface area of the completely separated phases is the ground state. This global equilibrium state, however, may require some time to reach when an energy barrier is formed, preventing the droplets from merging even when in direct contact. Such barriers, and the associated emulsion metastability, could be due to ionic double layers or steric repulsion of brush-like tails in non-ionic systems. In the rare cases when such a barrier is high, but the effective surface tension very low, a system forms inflated or deflated vesicles [3–5].

The situation may change if an additional physical field comes into the problem, bringing along its own energy and entropy contributions. The simple example studied in this work is the orientational order when one of the two emulsified fluids is a nematic liquid crystal. This question, when a nematic liquid crystal is the continuous majority phase with surfactant-covered fluctuating interfaces inducing bulk curvature deformations of the director, has recently attracted much attention,

*Corresponding author. Email: emt1000@cam.ac.uk

Liquid Crystals
ISSN 0267-8292 print/ISSN 1366-5855 online
http://www.tandf.co.uk/journals
DOI: 10.1080/02678290412331328009

generating a large literature on the topic of surface tension and wetting of nematic interfaces. Here we address the opposite end of the problem, when the isotropic continuous phase (water, in most cases) has small droplets of nematic liquid crystal dispersed in it. Surfactant is needed, as usual, to reduce the interface energy and also to impose strong anchoring boundary conditions for the nematic director. The basic finding of this work is that there is an additional contribution related to the elastic energy of topological defects in the confined nematic droplets, that creates a significant barrier for the droplet coalescence and leads to a new effect—topological stability of macroemulsions [6].

Droplets of nematic liquid crystal in an isotropic fluid, and the related topological defect structures, have been extensively studied before. One of the earliest significant contributions to this field was from Volovik and Lavrentovich [7]. Since the development of polymer dispersed liquid crystals [8], much more work has been done in this area [9]. However, in all cases the properties and effects of individual droplets have been addressed. Interesting physical effects here stem from the topological constraint, imposed on the director field in a closed volume by the anchoring condition on its surface [7], leading to topological defects of total point charge (+1) for a nematic and more complex structures in other phases.

The first studies of collective properties and aggregation of mobile nematic droplets in an isotropic suspending matrix (usually water) [6, 10] clearly demonstrated that the droplet coalescence is significantly hindered in the nematic phase. Spectacularly, samples of densely packed nematic emulsions studied in 1994 [6], after several years are still intact in our laboratory. On the other hand, if the droplets are heated above the nematic–isotropic transition, the coalescence of the whole sample occurs within a few seconds. This indicates that the surfactant coverage is not the encapsulation mechanism; but the nematic ordering inside the droplets is the key factor, providing the barrier for coalescence.

Figure 1 illustrates the point. Each nematic droplet contains a topological point charge of (+1); the sketch gives the example of a radial monopole that results from the perpendicular (homeotropic) anchoring at the boundary. If two droplets attempt to join, the resulting single simply-connected bounded nematic volume must have just one (+1) point defect, according to the basic topological rules, see [11] for detail. Unless one invokes some unlikely long range interaction that brings both (+1) defects in each droplet to the point of contact at exactly the right moment of time, allowing them to simultaneously undergo the required transformations, we have to assume that these two defects remain initially unaffected by the droplets merging. Hence, in between, another defect with point charge (−1) must be born and then annihilated with one of the two initial (+1) monopoles. This defect could be, as one can see from the figure 1 (*b*), a ring of the wedge disclination with the *linear* charge (−1/2) on the tip of the neck connecting the two droplets.

There is more than one late stage scenario for pair coalescence. One possibility is that the ring detaches itself from the surface, when the curvature of the neck decreases, and transforms into a hyperbolic monopole structure with point charge (−1), which then drifts into the volume towards one of the radial monopoles. The other is that the (−1/2) ring remains as a surface disclination and one of the point defects moves towards and disappears on the surface. This choice is curious but is of little relevance to the encapsulation phenomenon; what is important is that in order to form the initial neck the system must create an accompanying total (−1) point charge in isolation, at a distance $\sim R$ (the droplet radius) from other defects. This costs a macroscopic elastic energy $\Delta \sim KR$ (with K the characteristic value of the Frank elastic constant), while the gain due to the surface tension is minimal as the total area of the 'dumb-bell' is initially the same as of the two separate droplets. The elastic energy barrier for droplet coalescence Δ is proportional to the square of the nematic

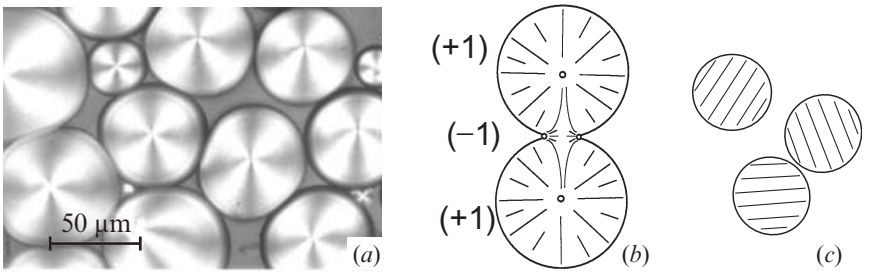

Figure 1. (*a*) A group of tightly squeezed nematic droplets in water matrix, viewed between crossed polarizers to reveal the radial director distribution, from [6]. (*b*) A sketch of topological defect balance on the attempted droplet coalescence. (*c*) Small droplets are not topologically charged ($WR/K << 1$) and should coalesce.

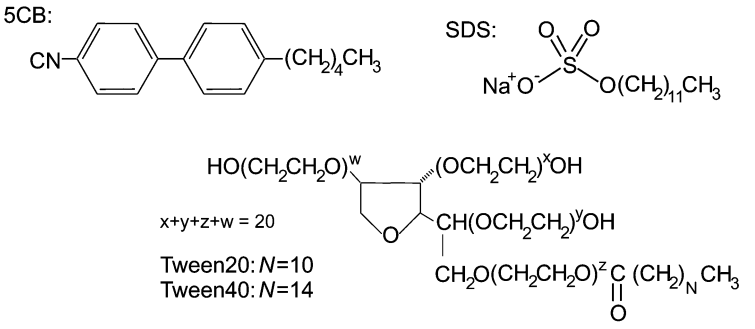

Figure 2. The chemical structures of the materials used. The scheme demonstrates the ionic surfactant nature of SDS and the non-ionic nature of Tween20 and Tween40, which differ only in the relative size of the hydrophilic head group.

order parameter Q, via $K \propto Q^2$, and disappears in the isotropic phase.

The other important factor in this argument is the overall topological state of nematic droplets. The singularities of nematic director field only arise when the anchoring on the droplet surface is strong enough, so that the system 'prefers' to pay an elastic energy for the topological defect, instead of violating the boundary conditions. The director anchoring energy W is a small anisotropic correction to the main surface tension and, typically, is proportional to the linear power of nematic order parameter Q. The characteristic parameter WR/K controls the state of the droplet: at weak anchoring or in very small droplets, when the condition $WR/K \ll 1$ holds, one has no topological defects, but instead droplets preserve a uniform director in the bulk, figure 1 (*c*). There is no additional barrier for coalescence of such droplets and their average size should grow until the topologically charged regime $WR/K \geqslant 1$ is reached, figure 1 (*b*). Accordingly, one expects the equilibrium distribution of droplet sizes to be skewed, with nearly all small droplets (of sizes below $R^* = K/W$) eventually disappearing altogether. For a typical thermotropic nematic liquid crystal $K \sim 10^{-11}$ N. The anchoring energy W is much less universal and is obviously system dependent; for a homeotropic anchoring on glass covered with a surfactant with a 14–16 atoms long hydrophobic tail, the literature gives $W \sim 10^{-5} - 10^{-6}\,\mathrm{N\,m^{-1}}$. From this one can estimate the characteristic droplet size $R^* \sim 10$–$100\,\mu\mathrm{m}$ and the energy barrier per particle $\Delta^* \sim 10^{-16}$ J. This barrier is very much greater than the typical energy of thermal fluctuations, at room temperature $k_B T \sim 4 \times 10^{-21}$ J, and thus topological stabilization of nematic emulsions should be significant.

In this paper we study the evolution of droplet size distribution in some detail. We focus on the experimental techniques and the data analysis that should be used to derive the expected skewed, non-symmetric size distributions and attempt to match the results with the basic analytical model taking into account the abrupt change of encapsulation barrier at $R \sim R^*$.

2. Emulsion preparation and characterization

2.1. *Sample preparation*

A series of oil in water (o/w) emulsions were created using 4-*n*-pentyl-4′-cyanobiphenyl (5CB, a common thermotropic nematic liquid crystal) as the oil phase, supplied by Sigma-Aldrich at 98% purity. The nematic to isotropic transition of 5CB is $T_{NI} \approx 35^\circ$C and the mean refractive index is $\bar{m} = 1.5320$[†]. The surfactants used were SDS (sodium dodecyl sulphate), Tween 20 (polyoxyethylene sorbitan monolaurate) and Tween 40 (polyoxyethylene sorbitan monopalmitate) supplied by Sigma. Figure 2 and table 1 present information about the ingredients. All solutions were made using deionized water.

Separate base solutions were made of each surfactant in water at a concentration $100\times$ the critical micelle concentration (cmc). Base solutions at $1\times$, $10\times$ and $50\times$ the cmc for each surfactant were then made by dilution. At room temperature 0.3 g of 5CB was added to 1.2 g of surfactant solution making a disperse phase volume of 20%. These macroscopically phase separated systems were emulsified using a Branson Sonifier 250. Care was taken not to exceed the nematic to isotropic transition, as it is known that emulsion droplets coalesce rapidly in the isotropic phase. The samples were kept sealed at room temperature.

2.2. *Sample kinetics*

The evolution of droplet size with time was monitored using a Malvern Mastersizer 2000 in conjunction with a small volume dispersal unit, Hydro 2000SM. An in-software general purpose model was used to produce

[†] Data from Sigma catalogue.

Table 1. Characteristic parameters of the three surfactants used in this work (with the source references): the hydrophilic–lipophilic balance (HLB), which is a measure of surface energy reduction of the oil/water interface with surfactant aggregated on it, and the critical concentration (CMC) of surfactant in water, at which the micromicelles are formed.

Surfactant	HLB	CMC ($mg l^{-1}$)
SDS	40 [12]	236 [12]
Tween20	16.7[a]	72 [12]
Tween40	15.6[a]	35 [13]

[a]Sigma catalogue

droplet size distributions from the scattering data. This required the values of both average refractive indices of the 5CB, $\bar{m}=1.5320$, and supernatant, $m_w=1.333$, the absorption value was set to 0.0. The model gives a log-normal distribution of particle sizes, and does not address local anisotropy in refractive index or other complicating factors, such as the skewed, non-symmetric size distribution (which we expect in this system, see below). This technique was not used to generate qualitative information, but only to indicate when the sample had reached a stable size distribution. A typical observation protocol included obtaining the Mastersizer data from small portions taken from the same sample shortly after preparation, then after 5, 7 and 12 days, and then after 11 and 14 weeks to verify that no further evolution takes place.

2.3. *TEM observation of individual droplets*

In this case we need to increase the number of droplets in the field of view. After light centrifugation, one drop of each concentrated emulsion of sample was placed onto a carbon support film (on a copper grid) and gently washed with methylamine tungstate negative stain solution for a few seconds. The films were blotted by placing a filter paper on the edge of the grids until an even film of stain could be seen remaining on the surface. The films were then left to dry naturally. The grids were examined and imaged in a Jeol 1200 EX Mk 2 transmission electron microscope operated at 80 kV.

Naturally, the preparation of grids creates a very different environment for the nematic droplets, compared with that in an original emulsion. Evaporation of excess water squeezes the droplets tightly together, forming an effectively cellular structure with the stain aggregating on interfaces. This observation technique, albeit only qualitative, gives an indication of characteristic droplet sizes (at very small length scales) and confirms the strong barrier for their coalescence, figure 3. As mentioned before, if we increase the temperature of the grid sample above $T_{NI}\approx 35^{\circ}C$, all cells coalesce within a few seconds.

2.4. *Optical microscopy and image analysis*

A Leica DMR optical microscope was used with a $100\times$ oil immersion lens in bright field, crossed polarizer and quarter-wave plate mode. For the subsequent image analysis it was essential that nematic droplets form a single layer sedimented at the bottom of the observation cell (sample holder). To achieve this, aliquots of each stored sample were diluted tenfold and placed inside a 50 μm spacer between a glass slide and a cover slip. Several micrographs were taken in each mode to ensure the whole sample was represented; images were captured by a linked computer. The micrographs were taken of this bottom layer after some time to allow for sedimentation. Bright field images were used to measure particle diameters in the image analysis software KS400. Table 2 gives the number of particles measured and the bin size used when comparing the image analysis data to the theoretical distribution of the data for each sample type.

Figure 4 gives an example of two emulsions, one with successful topological stabilization and the other with clearly less. It appears that in the emulsion with the director anchoring provided by the 12-carbon long tails of SDS the critical radius R^* is in the range of ~ 5 μm.

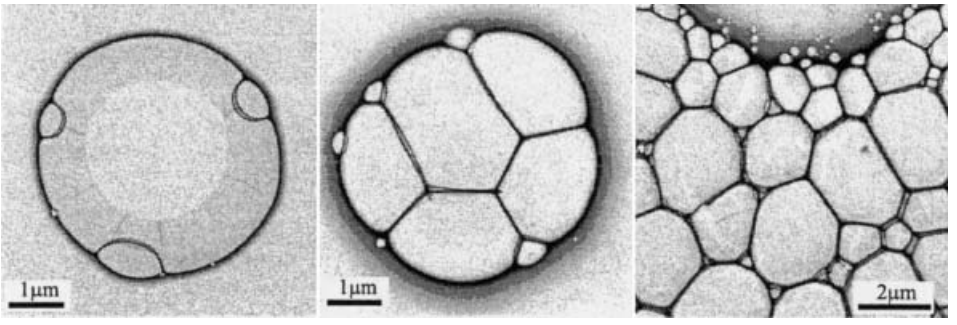

Figure 3. The TEM images of individual nematic droplets and packed groups of such droplets (see text for detail of staining and contrast).

Table 2. Statistics of microscopic image analysis on different samples: the number of droplets measured in images and the bin size to produce a distribution.

Solution	Number of droplets	bin size/μm
1 × CMC SDS	864	0.3
10 × CMC SDS	723	0.3
50 × CMC SDS	597	0.4
100 × CMC SDS	393	0.3
1 × CMC Tween 20	219	0.3
10 × CMC Tween 20	318	0.3
50 × CMC Tween 20	708	0.2
100 × CMC Tween 20	365	0.2
10 × CMC Tween 40	492	0.4
50 × CMC Tween 40	648	0.3
100 × CMC Tween 40	810	0.2

The 11-carbon tail and a much bulkier hydrophilic head of Tween 20, at its relatively low concentration in the base solution, appears insufficient to provide a strong coalescence barrier and a definite emulsion size selection. Overall, polarized microscopy images of a large number of emulsions indicate that droplets with maltese crosses (i.e. a radial (+1) monopole in the centre due to the homeotropic anchoring on their surface) are dominant in Tween emulsions as well, only at a much higher concentration of surfactant. In particular, the Tween 40 emulsion above 50 cmc has almost the same visual appearance as the SDS image in figure 4 (*a*). A more detailed analysis of droplet statistics also suggests that a large number of very small droplets survive in both Tween 20 and 40 emulsions, figure 5. It is important to keep in mind that the analysis of optical microscopy images is vulnerable to the small length cutoff, of about 0.5 μm, so we can only say reliably that the small sized droplets are absent in the equilibrated SDS emulsion.

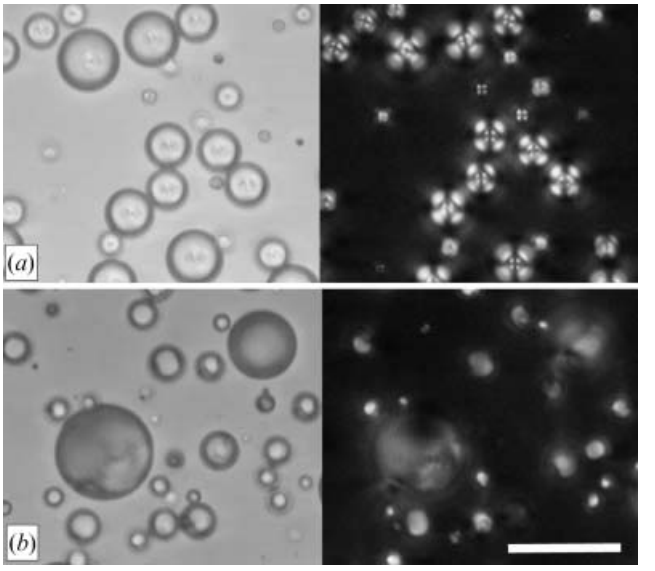

Figure 4. Optical microscope images, straight and between crossed polarizers, of (*a*) the 50 cmc SDS emulsion and (*b*) the 10 cmc Tween 20 emulsion. The SDS-based emulsion has a more uniform droplet size distribution and radial monopole director alignment, evident by the maltese crosses in polarized images. In contrast, the non-ionic Tween 20 emulsion has a broader size distribution and a much less definite director alignment. The bar represents 20 μm scale for all images.

The alternative technique, with the opposite limitation of ignoring droplets of large size but reliably taking into account the smaller objects, is light scattering.

3. Light scattering analysis

Small angle light scattering (SALS) was employed to provide an alternative quantitative measure of the droplet size distribution. In his case one needs as low concentration of droplets as possible, to remain reliably in the single-scattering regime. Accordingly, the small

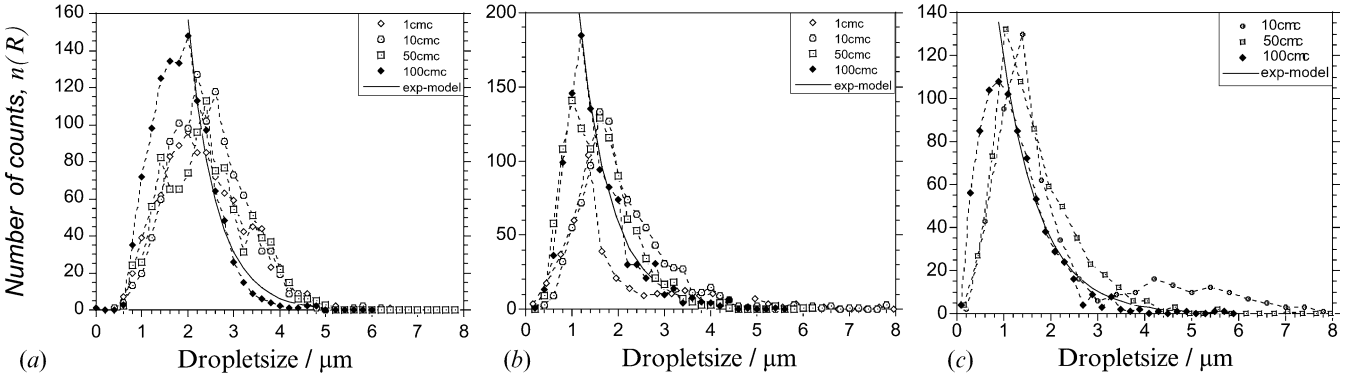

Figure 5. Droplet size distributions obtain from image analysis of microscope imaging. (*a*) SDS emulsion, (*b*) Tween 20 and (*c*) Tween 40, all at different concentrations of surfactant in the supernatant. The solid line in all three plots represents the fit by a simple exponential, see equation (3).

portions of each stored emulsions were diluted by ~500–1000 times. Samples were then made by containing a drop of such diluted materials at room temperature between two glass coverslips (thickness 0.17 μm) in the centre of a round 100 μm thick spacer (diameter 4 mm). The SALS camera consisted of a 0.5 mW He-Ne laser beam producing a collimated beam with a Gaussian profile of diameter ~1 mm, passing through a 1 mm aperture. The scattering pattern of the beam passing through the sample was projected onto a greyed glass screen on which a beam-stop was placed to obscure the directly transmitted beam. A Photonic Science Fast Digital Imager CCD camera, equipped with a zoom lens focused on the screen, was connected to a PC with a frame grabber to capture the scattering pattern. The camera was used at a maximum zoom to optimize the angular resolution of the scattering pattern. The frame-grabber was controlled by Photolite image processing and analysis software. Samples were diluted until a monotonic decrease was seen in the scattering pattern, thus indicating the single scattering regime; the exposure time was 100 ms. A 25 μm pinhole was used to calibrate the scattering patterns. The 2D scattering patterns were azimuthally averaged to produce functions of intensity against scattering vector q.

The analysis of small angle light scattering results can be notoriously cumbersome. Even if we ensure (as done in this work, by diluting the samples to a very low concentration of nematic droplets) that only the single scattering takes place, with the structure factor $S(q)=1$, the asymmetric particle size distribution makes the problem non-trivial. Briefly reviewing the basics [14], the single sphere of the size R has the scattering form-factor

$$P(q, R)=\left\{\frac{3}{(qR)^3}[\sin(qR)-qR\cos(qR)]\right\}^2 \qquad (1)$$

assuming that a small nematic droplet has a uniform average refractive index. The corresponding intensity $I(q, R)\propto P(q, R)$ falls rapidly with increasing scattering vector q and is very low after the first zero of (1), at $qR\approx 4.5$, see figure 6 (*a*). The real, observable scattering intensity distribution $I(q)$ is obtained by a convolution of the form-factor $P(q, R)$ with the particle size distribution—in effect, adding the contributions from each individual droplet:

$$I(q)\propto\langle P(q, R)\rangle=\frac{\int_0^\infty n(R)m(R)^2P(q, R)\mathrm{d}R}{\int_0^\infty n(R)m(R)^2\mathrm{d}R} \qquad (2)$$

where $m(R)\propto R^3$ is the molar mass of the scattering object and $n(R)$ the size distribution. From these qualitative theoretical arguments and the shape of the $n(R)$ tail found by the analysis of optical microscopy images, figure 5, we expect this distribution to be skewed. The inset of figure 6 (*b*) shows the model distribution, given by the normalized expression

$$n(R)=\frac{1}{R_s^2\xi+2R_s^2\xi+2\xi^3}\exp[-(R-R_s/\xi)],$$
$$\text{for } R>R_s. \qquad (3)$$

Here the cutoff radius R_s has the meaning of critical radius $R^*=K/W$ discussed above and ξ is the width of the distribution. One could assume it to be of the same order of magnitude but a little smaller, $\xi\sim 0.25R_s$, because the largest droplet that could form after a single collision of two droplets just below R^* each is about $2^{1/3}R^*$ in radius. The tail of the $n(R)$ distribution at larger sizes is due only to the biggest droplets growing slowly by incorporating the increasingly depleted population of very small ones.

The details of the following integration, equation (2), are quite tedious. The outcome depends on the relative

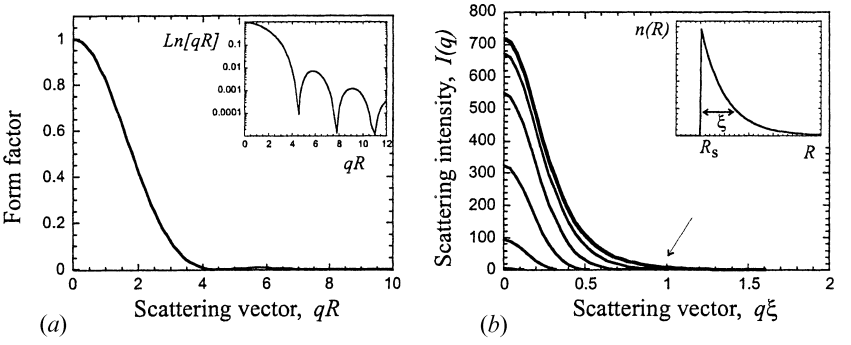

Figure 6. (*a*) The normalized form factor $P(q, R)/P(0, R)$ of individual droplets, plotted against the scaled wavevector qR; the inset shows the logarithmic representation highlighting the zeroes of $P(q, R)$. (*b*) The average intensity $I(q)$, from equation (2), in arbitrary units, plotted against $q\xi$. The decreasing curves correspond to $R_s=0.1\xi$, 4ξ, 5ξ, 7ξ and 10ξ, respectively. The inset shows the model size distribution $n(R)$ with the cutoff R_s and width ξ.

value of scattering vector, qR_s. The argument of the convolution integral in (2) has a pronounced first maximum, at

$$R_{\text{saddle}} \approx \frac{5}{4q^2\xi}\left[-1+\left(1+\frac{48}{5q^2\xi^2}\right)^{\frac{1}{2}}\right].$$

The integral is dominated by the region of small wave vectors, where $R_{\text{saddle}} \to 6\xi$. If the lower limit of this integral, R_s, is below this saddle-point, the resulting average scattering profile $I(q)$ is practically independent of the cutoff size R_s and terminates, roughly, at $q\xi \approx 1$, see figure 6 (*b*). If $R_s > R_{\text{saddle}}$, then only a portion of the relevant integrand is included in the final result and the scattering intensity $I(q)$ drops more sharply with q and terminates, roughly, at $qR_s \approx \frac{3}{2}$. To summarize: the effect of the skewed particle size distribution with a cutoff, equation (3), is to make the observed average light scattering intensity drop rapidly on increasing the scattering vector and not have the usual tail past $qR_s > 1.5$.

Experimental results on SALS for our three surfactant systems are shown in figure 7. Although unfortunately, very small scattering angles cannot be resolved (the beam stop is placed at $0.3\,\mu\text{m}^{-1}$ in all plots), the general features of the model distribution $I(q)$ are reproduced for SDS and Tween 40. It is important to emphasize a feature which is difficult to appreciate from the data representation in figure 7 and which is highlighted in the insets. The intensity $I(q)$ does not gradually decay but, for the droplet size distribution under consideration, drops to zero abruptly, with a very definite cutoff q. The arrow points at this cutoff wave vector in the insets for SDS and Tween 40, while it is evident that for Tween 20 the intensity is, in fact, gradually decaying. Note that at lower surfactant concentration all emulsions appear to have their droplets grow significantly (hence the scattering intensity $I(q)$ confined to progressively smaller wave vectors).

If we interpret the intensity cutoff in experimental plots as the position where $qR_s = 1.5$, the estimate of the critical droplet size obtained for the emulsions formed at the high concentration of each surfactant becomes: $R^* \sim 0.3\,\mu\text{m}$ for SDS and $R^* \sim 0.8\,\mu\text{m}$ for Tween 40, while for Tween 20 there is no evidence of a cutoff.

4. Conclusions

Apart from the demonstration of topological stability of nematic macroemulsions in different surfactant solutions, the main practical implication of this work is the approaches to their analysis. Few of the traditional methods of particle sizing are applicable here because of the expected non-symmetric (skewed) nature of their size distribution. Since the key characteristics of such systems, the critical radius $R^* = K/W$, is expected to be in the range of single microns, optical microscopy is not the optimum technique and the method of choice then becomes light scattering. Here much remains to be understood and, once again, the traditional analytical tools are not applicable (as they are all based on the normal distribution or a superposition of several such distributions). We went only a few initial steps along this road, relying on our analysis of experimental $I(q)$ and on the model size distribution $n(R)$ given in equation (3), motivated by the optical measurements. This assumption is the weakest aspect of our analysis and it will have to be re-examined as more data and, perhaps, a more detailed kinetic model of particle coalescence in the presence of a topological barrier would suggest a better size distribution.

In practical terms, of particular interest is the control over the equilibrium droplet size R^* through the choice of surfactant (affecting W) and nematic material. The

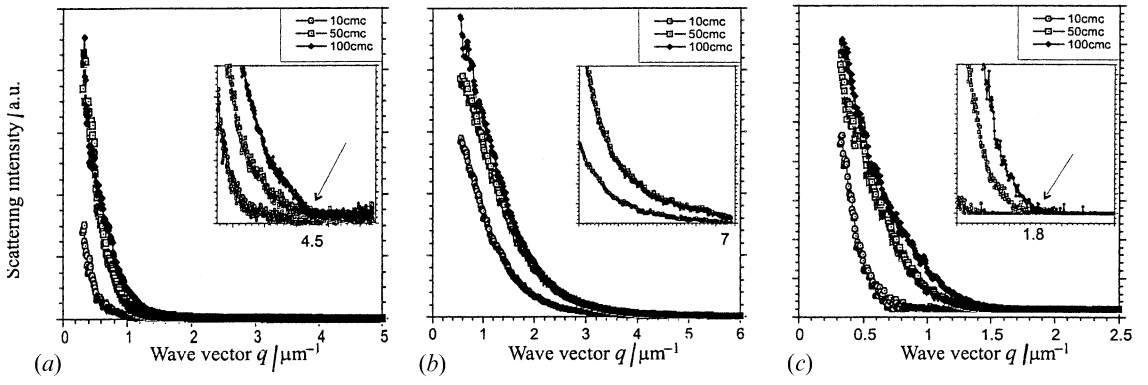

Figure 7. Small angle light scattering intensity profiles, $I(q)$ for: (*a*) SDS emulsion, (*b*) Tween 20 and (*c*) Tween 40; all at different concentration of surfactant in the supernatant, labelled on plots. The arrow marks a wave vector q, where we estimate the scattering intensity to be effectively cut off.

ability to switch off the mechanism of stabilization, by taking the material confined in droplets into the isotropic phase, is also of great importance. One can imagine, among many other possibilities, that a possible application could use the polymerization of surfactant to form a percolating sponge with mesh size controlled by K/W.

Acknowledgement

This research has been initiated and supported by Unilever Plc.

References

[1] D.A. Weitz. *Nature*, **410**(6824), 32 (2001).
[2] J. Bibette, D.C. Morse, T.A. Witten, D.A. Weitz. *Phys. Rev. Lett.*, **69**, 2439 (1992).
[3] P. Becher. *Emulsions: Theory and Practice*. Reinhold, New York (1965).
[4] J.H. Clint. *Surfactant Aggregation*. Blackie, Glasgow, London (1992).
[5] J. Bibette, F. Leal-Calderon, V. Schmitt, P. Poulin. *Emulsion Science*. Springer, Heidelberg (2002).
[6] E.M. Terentjev. *Europhys. Lett.*, **32**, 607 (1995).
[7] G.E. Volovik, O.D. Lavrentovich. *Sov. Phys. JETP*, **58**, 1159 (1983).
[8] S. Zumer, A. Golemme, J.W. Doanne. *J. opt. Soc. A*, **6**, 403 (1989).
[9] F. Xu, H.S. Kitzerow, P.P. Crooker. *Phys. Rev. A*, **46** 6535 (1992); P.S. Drzaic, A. Muller. *Liq. Cryst.*, **5** 1467 (1989).
[10] P. Poulin, D.A. Weitz. *Phys. Rev. E*, **57**, 626 (1998).
[11] G.E. Volovik. *The Universe in a Helium Droplet*. Clarendon Press, Oxford (2003).
[12] A.A. Chambers, J. Rickwood (Eds), *Biochemistry Lab Fax*. Blackwell Scientific, Oxford (1993).
[13] S. Fleisher, L. Packer (Eds), *Methods in Enzymology*. Vol. LVI, Academic Press, London (1979).
[14] J.S. Pedersen. *Adv. Coll. Int. Sci.*, **70**, 171 (1997).